NeuroImage 82 (2013) 1–12

Contents lists available at SciVerse ScienceDirect

NeuroImage

journal homepage: www.elsevier.com/locate/ynimg

Diffusion imaging quality control via entropy of principal direction distribution

Mahshid Farzinfar [a,*], Ipek Oguz [a,b], Rachel G. Smith [b], Audrey R. Verde [a], Cheryl Dietrich [a], Aditya Gupta [a,e], Maria L. Escolar [e], Joseph Piven [a,b], Sonia Pujol [f], Clement Vachet [a,b,d], Sylvain Gouttard [d], Guido Gerig [d], Stephen Dager [g], Robert C. McKinstry [h], Sarah Paterson [i], Alan C. Evans [j]
The IBIS network, Martin A. Styner [a,b,c]

[a] Department of Psychiatry, University of North Carolina, Chapel Hill, USA
[b] Carolina Institute for Developmental Disabilities at University of North Carolina, Chapel Hill, USA
[c] Department of Computer Science, University of North Carolina, Chapel Hill, USA
[d] Scientific Computing and Imaging Institute, School of Computing, University of Utah, Salt Lake City, UT, USA
[e] Children's Hospital of Pittsburgh, University of Pittsburgh, Pittsburgh, PA, USA
[f] Surgical Planning Laboratory, Brigham and Women's Hospital, Harvard Medical School, Boston, MA, USA
[g] Dept. of Radiology, University of Washington, Seattle, USA
[h] Dept. of Radiology, Washington University, St. Louis, USA
[i] Department of Pediatrics, Childrens Hospital of Philadelphia, PA, USA
[j] McConnell Brain Imaging Center, Montreal Neurological Institute, Montreal, Canada

ARTICLE INFO

Article history:
Accepted 3 May 2013
Available online 17 May 2013

Keywords:
Diffusion magnetic resonance imaging
Diffusion tensor imaging
Quality assessment
Entropy

ABSTRACT

Diffusion MR imaging has received increasing attention in the neuroimaging community, as it yields new insights into the microstructural organization of white matter that are not available with conventional MRI techniques. While the technology has enormous potential, diffusion MRI suffers from a unique and complex set of image quality problems, limiting the sensitivity of studies and reducing the accuracy of findings. Furthermore, the acquisition time for diffusion MRI is longer than conventional MRI due to the need for multiple acquisitions to obtain directionally encoded Diffusion Weighted Images (DWI). This leads to increased motion artifacts, reduced signal-to-noise ratio (SNR), and increased proneness to a wide variety of artifacts, including eddy-current and motion artifacts, "venetian blind" artifacts, as well as slice-wise and gradient-wise inconsistencies. Such artifacts mandate stringent Quality Control (QC) schemes in the processing of diffusion MRI data. Most existing QC procedures are conducted in the DWI domain and/or on a voxel level, but our own experiments show that these methods often do not fully detect and eliminate certain types of artifacts, often only visible when investigating groups of DWI's or a derived diffusion model, such as the most-employed diffusion tensor imaging (DTI). Here, we propose a novel regional QC measure in the DTI domain that employs the entropy of the regional distribution of the principal directions (PD). The PD entropy quantifies the scattering and spread of the principal diffusion directions and is invariant to the patient's position in the scanner. High entropy value indicates that the PDs are distributed relatively uniformly, while low entropy value indicates the presence of clusters in the PD distribution. The novel QC measure is intended to complement the existing set of QC procedures by detecting and correcting residual artifacts. Such residual artifacts cause directional bias in the measured PD and here called dominant direction artifacts. Experiments show that our automatic method can reliably detect and potentially correct such artifacts, especially the ones caused by the vibrations of the scanner table during the scan. The results further indicate the usefulness of this method for general quality assessment in DTI studies.

Introduction

Diffusion magnetic resonance imaging has become an increasingly relevant neuroimaging technique because of its ability to investigate microstructural features of white matter non-invasively and in-vivo, particularly in studies of normal, developing, aging and pathological human brain (Bach et al., 2011; Hsu et al., 2008; Johansen-Berg and Rushworth, 2009; Le Bihan et al., 1986; Solano-Castiella et al., 2010; Unrath et al., 2010). Within the brain, diffusion of water molecules inside the tissues differs from "Brownian motion" and reflects interactions of molecules with many obstacles such as cell membranes, fibers and macro molecules. Diffusion Tensor Imaging (DTI) measures the rate and directionality of water displacement in various brain tissues via a Gaussian model of diffusion. The tensor in DTI is estimated using a set

* Corresponding author.

1053-8119/$ – see front matter © 2013 Elsevier Inc. All rights reserved.
http://dx.doi.org/10.1016/j.neuroimage.2013.05.022

of diffusion sensitized MR images, known as Diffusion Weighted Images (DWIs), by using several (at least six) non-collinear diffusion sensitizing gradients (Basser et al., 1994). Several tensor properties are commonly employed to analyze DTI, such as Fractional Anisotropy (FA) and PD, which characterize the shape and the principal direction of the resulting tensor. As of late, plenty of research has been conducted regarding diffusion tensor models resulting in several useful estimation techniques such as linear least square (LLS), non-linear least square, weighted least square (WLS) based on the log Rician probability distribution (Salvador et al., 2005) and Maximum Likelihood estimate using log-likelihood function of the Rician distribution (Fillard et al., 2007). While the use of the tensor model is currently predominant in clinical applications of diffusion MRI, DTI is unable to characterize fiber crossing within a voxel. Consequently, the need for investigating the non-tensor models has increased particularly for tractography (Basser et al., 2000; Mori et al., 1999) and fiber-driven analysis.

As theoretical work characterizing DTI grows, it is essential to increase their practical usability from a clinical environment perspective (Pierpaoli and Basser, 1996; Tournier et al., 2011). Inherently, DWI images suffer from diverse artifacts as a result of limitation or malfunction in the hardware or software of the scanning device. In addition, severe artifacts may also originate from physiological noise such as bulk head motion or respiratory motion. These difficulties cause propagated bias of diffusion tensor property estimation. Thus, it is essential to establish appropriate image quality assessment techniques on both DWI and DTI data.

DWI-based image quality control techniques can detect and potentially correct artifacts such as inter-slice abrupt differences in signal intensities, venetian-blind (Liu et al., 2010), eddy current induced distortion (Andersson and Skare, 2002; Reese et al., 2003), susceptibility (Andersson et al., 2003; Jezzard et al., 1999) and drop-out signal intensities (Tournier et al., 2011) which can be caused by mechanical vibration artifact (Gallichan et al., 2010) (see Fig. 1). The standard approach to correct drop-out, venetian-blind and inter-slice change based artifacts is to exclude the affected DWI images prior to the DTI estimation (Liu et al., 2010). It is noteworthy that such correction via exclusion of DWIs can lead to a biased estimate of the resulting tensor's properties and principal direction.

In order to reduce the influence of artifacts and the inherent noisy characteristics in DWIs, methods for denoising DWI or DTI data have been proposed (Tristán-Vega and Aja-Fernández, 2010) based on joint information from all DWIs and the correlation between them to filter the DWI images. Another possibility is to apply regularization of tensor images, in addition to estimating the tensor model (Wang et al., 2004). Alternatively, a maximum-a-posterior framework estimation can be used to couple tensor estimation and regularization to better capture information from noisy images (Fillard et al., 2007). Additionally, methods have been proposed that detect and reduce the influence of outliers as part of an iterative DTI estimation process that gives lower weights to artifactual data (Chang et al., 2005).

While these approaches are applicable in many general DTI settings, they may fail for more systematic artifacts resulting from mechanical vibration. These artifacts are known to occur mostly in some 3 Tesla Siemens scanners for subjects weighing less than 30 kg. Although the pre-processing hardware fix described in Liu and Liu (2011) corrects some of these artifacts, a substantial number of subjects remain artifactual. Strong diffusion gradients cause low-frequency mechanical resonance of the diffusion MRI system (Hiltunen et al., 2006; Mukherjee et al., 2008). This low frequency mechanical resonance leads to uneven distribution of vibrations within parts of the scanner and patient table, and hence uneven brain tissue movement. These vibration artifacts present as an area of signal loss in the DWIs and a subsequent directional bias in the estimated tensors. The directional bias is visually evident in color-coded FA images with local orientation of the principal tensor direction (see Fig. 2). The vibration artifact is hypothesized to be mainly due to substantial local echo shift in k-space, which exceeds the k-space window (Mohammadi et al., 2011). The movement-related signal-loss occurs most likely due to physical resonance of the scanner with longer time vibration when it is excited by strong left-right gradients (Gallichan et al., 2010). Therefore, not only the quality of DWIs is affected, but also the diffusion-related measurements are disrupted.

As a post-processing step of quality control to correct vibration artifacts, an improved DTI estimation approach was proposed (Gallichan et al., 2010). A co-regressor is used based on an empirical approximation to influence the artifacts in diffusion-tensor fit. This approximation assumes that the artifacts result from diffusion gradients in the left–right direction and also using the co-regressor restricts performance of correcting these artifacts. More recently, as a systematic technique for correcting these artifacts (Mohammadi et al., 2011), an approach was proposed using phase-encoding (PE) reversal by combining two images with reversed PE direction, each weighted by a function of its local tensor fit error. The disadvantage of this approach is that systematic correction causes limitations and difficulties during image acquisition which makes it less applicable.

In this work, we investigate artifacts that introduce a directional bias in the measured principal direction of diffusion (see Figs. 2 and 3), called dominant direction artifacts in the remainder of this paper. Upon visual inspection, such artifacts may be apparent in DWIs as local signal intensity drop-out or may not be apparent in DWIs. We propose a novel DT-MRI quality control measure to detect these artifacts by assessing the orientational bias of the diffusion tensor model and refurbishing DWIs using an entropy-based measurement on the orientational distribution of principal directions. The main difference between our approach and other vibration correction approaches (Gallichan et al., 2010; Mohammadi et al., 2011) is that these approaches adjust major vibration-induced drop-out signal intensities in DWIs. However, we show that these artifacts may not be visually apparent in DWIs. Thus, it would be

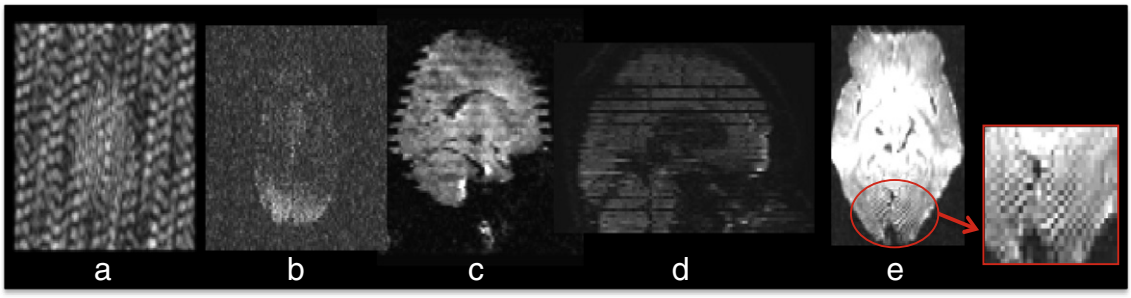

Fig. 1. Examples of intensity artifacts detected. (a) An electromagnetic interference-like artifact, (b) severe signal loss in the anterior and middle regions, (c) Venetian blind artifact, (d) inter-slice and intra-slice intensity artifact and (e) checkerboard artifact.

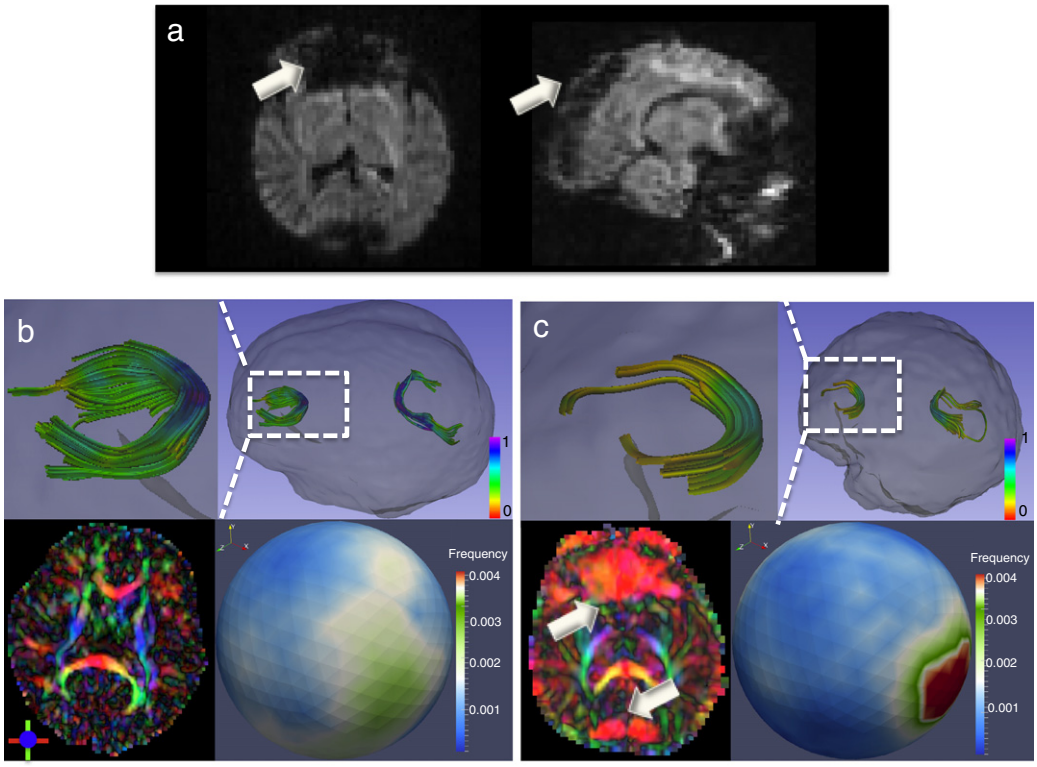

Fig. 2. Vibration artifact with local signal loss: (a) Axial and sagittal cross-sections of a diffusion-weighted image (diffusion gradient is [−0.86 0.43–0.24]) with local signal loss both in anterior (arrow on left image) and posterior (arrow on right image) medial regions. (b) Example of artifact-free scan with tractography results of the genu and splenium (top row), color-coded FA (bottom left) and corresponding spherical histogram of the PD distribution within the whole brain (bottom right). (c) DTI estimation of (a) and its PD histogram (same colormaps as in (b)). 3D Slicer tool is used for tractography using fiducial seeds.

necessary to inspect indirect identifiers such as DTI driven principal direction information. Our method is a complementary process to our existing, open-source DWI-QC tool, DTIPrep (Liu et al., 2010), which detects and corrects DWI artifacts such as inter-slice brightness artifacts, venetian blind artifacts, eddy current artifacts, within-DWI and between-DWI patient motion. The orientational distribution is computed via an icosahedron subdivision based spherical histogram of the principal directions within the following regions: total brain, wholebrain gray matter together with Cerebrospinal Fluid (CSF) and whole brain white matter. We demonstrate the performance of our approach in neonate, pediatric and adult studies. In addition, we inspect the stability of our approach in pathological studies that may affect the orientational distribution of the principal directions.

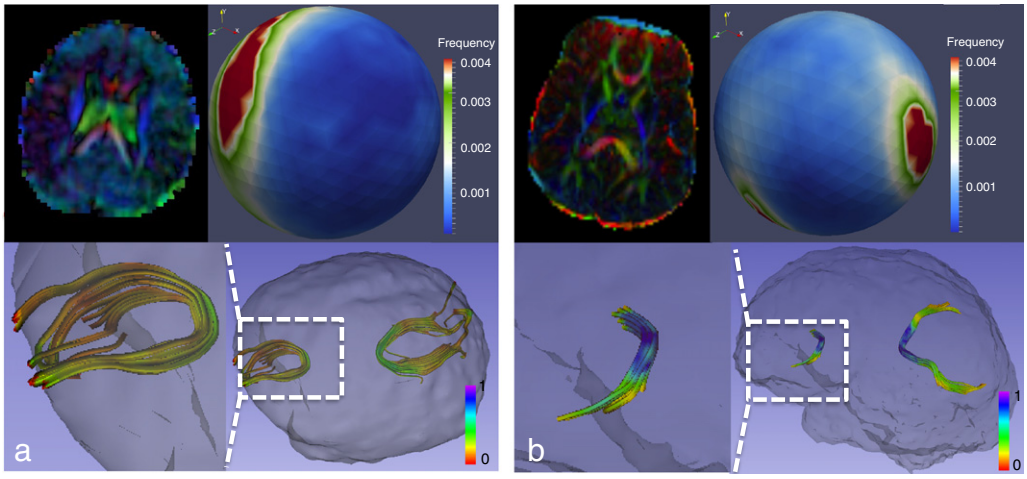

Fig. 3. (a) Superior-inferior/blue-colored artifact mixed with anterior-posterior/Green-COLORED artifact visible in the color coded FA (top left), tractography results of genu and splenium (bottom row) and the corresponding spherical histogram of the PD distribution within the whole brain (top right). (b) Left-right/red-colored artifact mixed with superior-inferior/blue-colored artifact with tractography results of the genu and splenium (bottom row), color-coded FA (top left) and the corresponding spherical histogram of PD distribution within the whole brain (top right, same colormaps as in Fig. 2).

Table 1
Summary of DTI protocol details.

Dataset	Scanner	Encoding direction	Non-DW images (b = 0)	Isotropic resolution (mm)	Trajectory of head circumference	b-value s/mm^2	#subjects
Pediatric 6 mo (IBIS)	Siemens Tim Trio	25	1	2	44	50–1000	298
Pediatric 12 mo (IBIS)	Siemens Tim Trio	25	1	2	44	50–1000	230
Adult (TRACK-HD)	Siemens Tim Trio	64	8	2.5	50	1000	80
Neonate (Krabbe)	Siemens Allegra	6 and 42	1 and 7	2	35	1000	11
Glioblastoma Grade 4	GE	31	1	2.6	50	1000	1

Materials and methods

Motivation: artifacts of dominating direction

The motivation behind this study is to identify a category of residual and pronounced artifacts remaining after standard DWI QC procedures. Mainly present in the DTI domain, this category of artifacts is characterized as dominant direction of diffusion. They can be detected visually by identifying either a local dominant color (see Fig. 2) or a widespread dominant color in a color-coded FA image (see Fig. 3). Fig. 2-b shows the anterior (genu) and posterior (splenium) fiber bundles of the corpus callosum (top) for an artifact-free scan (as determined by visual QC) along with its color-coded FA image (bottom-left) and orientational distribution of principal directions (bottom-right) within the whole brain region. The spherical principal direction distribution in an artifact-free environment displays some clustering due to the expected normal brain network anatomy while the dominant direction artifacts generally prompt a higher degree of clustering in the spherical principal direction distribution as seen in Figs. 2c and 3.

Artifacts identified by a local dominant color in FA images are most likely induced by DTI-related mechanical vibration (Gallichan et al., 2010; Hiltunen et al., 2006; Mohammadi et al., 2011) (see Fig. 2-c). Fig. 2-a shows an example of a volume that is affected by vibration artifact and anomalous signal loss regions in both anterior and posterior medial regions. Using standard DWI QC approaches, such regions are hard to detect as signal loss is not abrupt (i.e. from one DWI slice to another, or from DWI gradient to a directionally similar one). As the estimated tensor from such corrupted DWIs is directionally biased, a dominant red color can be observed in frontal and posterior lobes of FA images and corresponding tractography through affected regions can be significantly deformed (see Fig. 2-c). As mentioned above, the associated spherical principal direction distribution shows a heightened degree of clustering when compared to an artifact free scan.

Artifacts identified by a widespread dominant color also affect the DWIs, but the effect may not be above a noise level to a degree that could be detected visually. Fig. 3 shows two examples of widespread dominant green and red artifacts chosen from neonate and pediatric (12 month) cases respectively (see Table 1). Fig. 4 shows the corresponding DWIs, FA and MD images of the case shown in Fig. 3-b. For creating the color-FA image, 23 DWIs are used after excluding 2 affected DWIs by inter-slice abrupt differences in signal intensities through the standard automated DWI QC processing. As seen in Fig. 4, signal intensity dropout is not evident in the DWIs though visual inspection alone. Such artifacts become visually apparent on the color-coded FA images. Low magnitude vibration effects (e.g. after hardware fix) may shift the k-space center by some fraction of the k-space window, resulting in signal decrease but not a complete dropout. Thus, the gray matter regions suffer from this artifact more, as the diffusion signal is (relatively) isotropic. Therefore, only a small decrease in image intensity due to vibration is required to bias the primary eigenvector of the tensor toward the affected direction. Tractography results from such scans show a considerably deformed shape for most major fiber tracts. The principal direction distribution also shows a heightened degree of clustering to indicate the presence of the dominant direction artifact (Fig. 3).

Overview

Preprocessing

Since the proposed QC procedure is intended to complement the existing set of DWI-QC procedures, we first apply our standard DWI-QC using the tool DTIPrep (Liu et al., 2010).[1] This step helps remove DWI-based artifacts originating from motion, low SNR and malfunction in the hardware and software of the scanning device. DTIPrep uses an adaptable protocol to control the QC processing consistency within and across studies. Based on a defined protocol, the QC processing is employed as follows: 1) checking the image characteristics (space & size) and cropping the image, 2) checking the b-value and diffusion gradient vectors, 3) applying a Rician noise filter using the method adopted by (Tristán-Vega and Aja-Fernández, 2010), 4) checking for inter-slice brightness artifacts and venetian blind artifacts by evaluating correlation-intensities within slices and gradients, 5) rigid co-registration of all baseline (b = 0) images and computation of the average baseline image, 6) eddy current and motion correction using non-rigid registration to the average baseline image and 7) checking for residual motion via rigid registration to the average baseline. The required time is around 12 min for these processes. The post-QC image and prior tissue segmentation masks are used for DTI estimation via a weighted-least square fit (see Fig. 5).

Regional definition

The dominant direction artifacts affect locations of both isotropic and anisotropic diffusion. According to Gallichan et al. (2010), correlation between the measured signal and the left-right component of the diffusion gradients is significant within the splenium tract and cortical gray matter when vibration artifacts occur. In this research, we investigated the relative effect of dominant direction artifact through several measures: a) whole brain, b) gray matter including CSF and c) white matter. The corresponding regions were determined via automatic atlas-based tissue classification[2] (Prastawa et al., 2005) from additional structural T1 and T2 weighted MR images acquired during the same scan session as the DWI images. The segmentation result is mapped on the average baseline via rigid, affine and B-spline registration of the T2 weighted image in 3D Slicer[3].

Distribution of the Principal Direction (PD)

Following diffusion tensor computation via weighted least-squares estimation, the distributions of the tensor principal directions are computed as spherical histograms with bins defined by a quasi-uniform, icosahedron based spherical subdivision. Finally, the entropy of PD distribution is computed from the spherical histogram and compared with prior training data that defines the expected range of the entropy for artifact-free scans. A leave-one-out scheme

[1] http://www.nitrc.org/projects/dtiprep.
[2] http://www.nitrc.org/projects/abc.
[3] http://www.slicer.org.

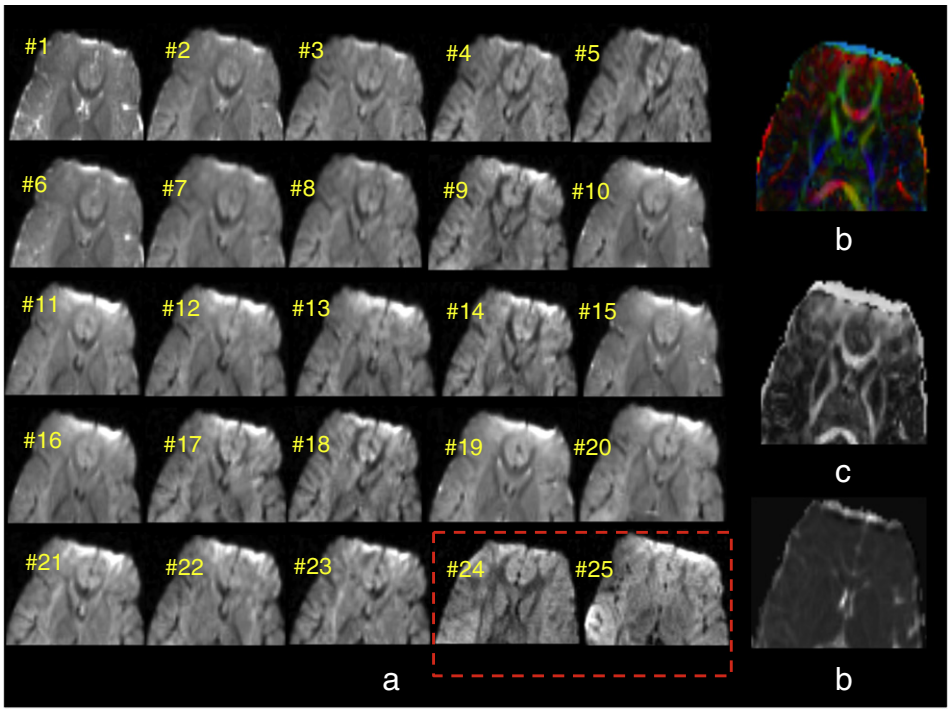

Fig. 4. Example of dominant directional artifacts with widespread manifestation from pediatric 12 month study with multiple b-values (50–1000) (see Table 1). It is seen that such artifacts may not be apparent in DWIs through visual inspection as drop-out signal intensities. The individual DWIs in axial view after excluding 2 affected DWIs (highlighted by red surrounding dashed line) by inter-slice abrupt differences in signal intensities through the standard automated DWI QC processing. All DWIs are displayed using the same intensity windowing. (b–d) The corresponding color-FA, FA and MD images, created from the DWIs in (a). They show that only the color-FA images demonstrate the artifacts visually through widespread dominant red color and neither FA nor MD information is useful for artifact detection. The obtained entropy value over whole the brain for this scan is 6.46 and its z-score is 2.29, which categorizes it into the unacceptable range.

is employed to correct the DWI set by excluding individual DWI images and to test for optimal improvement in the entropy values. Fig. 5 shows a schematic overview of our proposed DTI-QC approach. The details of this approach are discussed in the following sections.

Distribution of the Principal Direction (PD)

In order to represent the PD distribution, we employ a spherical coordinate system on which we compute the PD histogram. The spherical histogram bins are computed using a subdivision of the unit sphere. Two different subdivisions have been employed in the literature (Clarke, 2002). The first option subdivides the unit sphere based on spherical or geographical coordinates/angles (ϕ, θ), where a rectangular grid is defined as a uniform subdivision of longitudes (ϕ) and latitudes (θ) (Cui et al., 2011). However, such an angular coordinate grid is not optimal for the computation of spherical histograms (Clarke, 2002), as the actual size of the subdivision rectangular face area on the unit sphere varies widely from the equatorial to polar regions. The second common option for a spherical subdivision is the quasi-uniform icosahedron subdivision, in which the triangular faces of an icosahedron are linearly or recursively subdivided into smaller triangles whose vertices are projected to the unit sphere. While the icosahedron is uniform in spacing and area, the icosahedron subdivision is not, but can be considered a quasi-uniform spherical subdivision due to the relatively small variance in spacing and area, especially when compared to the above angular subdivision. While face-wise binning could be chosen for the spherical histogram, we chose the nearest-vertex based binning for the PD histogram due to its implementational simplicity. Using subdivision level 8, 812 bins are employed to reliably estimate the PD histogram from approximately 80,000 voxel-wise measurements within the brain in a common 2 mm isotropic resolution DTI dataset. While there are other approaches for deriving the samples on the sphere, such as the electrostatic repulsion model (Jones et al., 1999), the exact distribution of the bins is not crucial to the work since they are merely used as histogram bins for estimation the entropy; that is to say, any approximately even distribution of the samples is adequate. Additionally, the icosahedron subdivision method is faster and has a more straightforward implementation than the electrostatic repulsion method.

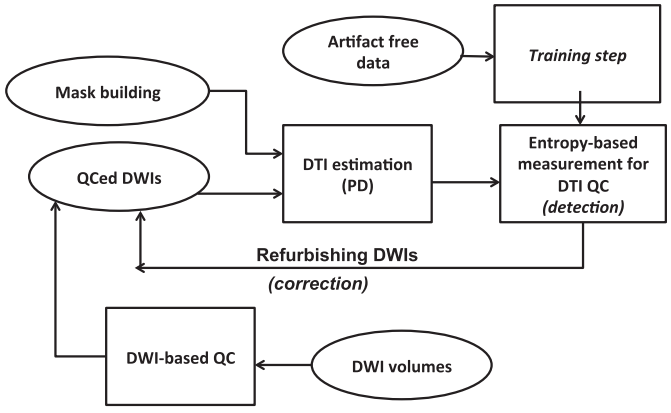

Fig. 5. A schematic overview of the proposed DTI-QC approach.

Orientational entropy for DTI-QC

One of the goals of our orientation based DTI-QC metric is to be independent from the patient's position in the scanner. We chose Shannon's entropy, a concept well known in information theory (Shannon, 2001), to summarize the PD distribution. In our application, the entropy of a distribution of PD represents the scattering and spread

of dominant direction within brain regions measured independent of alignment of the spherical parameterization. Higher entropy indicates that the PD' distribution is more uniform. Lower entropy demonstrates clustering of the PD distribution and a higher degree of such clustering is a consequence of the aforementioned artifact of dominant direction. Given the PD histogram, the proposed orientational entropy is defined as:

$$E = -\sum_{i=1}^{K} p_i log(p_i) \quad (1)$$

where K is the number of vertices/bins and p_i is the normalized frequency in the PD histogram at bin i.

Detection

In order to detect scans with an unexpected value of entropy (lower values of entropy for artifacts of dominant direction), we compare a given DTI scan's entropy to values learned from a prior set of artifact-free samples. We employ z-scoring to categorize the quality of a DTI scan into three categories: acceptable ($z < 1.64/90\%$), suspicious ($z \geq 1.64/90\%$) and unacceptable ($z \geq 2.58/99\%$). For our experiments, we evaluate the DTI quality within the whole brain, gray matter including CSF, and white matter.

Correction

For our correction step, we employed a simple, iterative leave-one-out-strategy over all individual DWI images by recomputing DTI images and corresponding entropies. At each iteration, the DWI with maximal improvement is removed and all leave-one-out entropies are recomputed. This process is continued until either the z-score is in an acceptable range or a maximum threshold for exclusion is reached. If the correction process is run on artifact free scans, the correction method would stop after one iteration as the entropy values of all leave-one-out steps would be scored as acceptable, and the tensor data would remain unchanged.

Experiments and results

We thoroughly tested our approach for robustness in a variety of populations such as pediatric, neonate, and adult human participants. In addition, we tested the performance of our approach on a set of scans with different brain pathologies. The summary of applied DTI protocols of these sets is shown in Table 1.

Dominant direction artifact detection in pediatric scans

The first experiments were performed on a population of 6 and 12 month old children scanned on Siemens Tim Trio 3T scanners at 4 different collaborating sites in the USA (University of North Carolina at Chapel Hill, Washington University, University of Washington and the Children's Hospital of Pennsylvania) as part of the IBIS (Infant Brain Imaging Study) network.[4] The acquisition protocol employs 25 non-collinear, uniformly spaced gradient directions at multiple b-values (ranging from b = 50 to 1000) at a resolution of 2 mm isotropic. Although both age groups were acquired with the same DTI protocol, each age group displayed a slightly different PD distribution due to the difference in the ratio of brain size to voxel resolution, which results in differences in partial voluming effects between the groups. Thus, we have trained the expected entropy values within each group separately.

Using visual QC, we found directional artifacts to be a serious concern in this pediatric study, especially in the scans of 6 month old participants, which mainly occurred as dominant red direction artifacts (along the medial-lateral direction). While some scans showed localized signal loss in the DWI images, many affected scans did not visually display this signal loss. However, the directional artifact became visible as a widespread red appearance in the color-coded FA images. For all 4 sites, the overall occurrence rate of directional artifacts was 1%, 5%, 54% and 12% respectively, which indicates a non-uniform occurrence of this artifact. We compared the results of the detection step of our approach to visual assessment by human expert raters (CD, RGS). Based on the degree of artifact appearance, scans were classified as Exclude (Ex), Borderline exclude (B-ex), Borderline include (B-in) and Include (In).

Fig. 6 shows the performance of our DT-QC approach on the scans of 6 and 12 month old participants according to the z-score of the orientational entropy values. The plots show the percentage of the detection process for each of the classifications within whole brain, gray matter including CSF, and white matter. For the training process in scans of 6 month old participants, we selected 77 artifact-free scans from a total of 298 scans. For the training process in scans of 12 month old participants, 81 artifact-free scans were selected from 230 scans.

For the 6 month age range scans, we observed considerable agreement in the whole brain region, Fig. 6-a, as all excluded cases scored within the unacceptable range, as well as all suspicious cases were classified as borderline exclude or borderline include. A small set of cases scored within the unacceptable range while being classified as include. Detection performance is slightly worse in the gray matter (Fig. 6-b) and considerably worse in the white matter only (Fig. 6-c) where several excluded cases scored within the acceptable range. This decrease in performance is primarily due to the varying degree of white matter segmentation accuracy across the scans, as tissue segmentation in the scans of 6 month old participants suffers from a lack of contrast between white and gray matter in the structural MR images. As structural contrast between white and gray matter is considerably better at 12 months old, the detection performance is clearly more consistent than in scans of 6 month old participants (see Fig. 6). Our DTI-QC entropy measurements within whole brain were able to detect 90.71% of “Exclude” and “Borderline Exclude” scans. In white matter regions, only 57.14% of “Exclude” and “Borderline Exclude” scans were detected. We will show that across both age groups, sensitivity and specificity of the detection process are acceptable for the whole brain region. It is noteworthy that all scans scored as “suspicious” indicate a need for further visual inspection and a significant number of scans scored within this suspicious range.

Moreover, to address the dominant direction artifacts, all four sites in this study adopted a hardware vibration fix recently devised by Siemens (Liu and Liu, 2011). The studied database consists of pre-fix and post-fix scans, though the pre-fix scans outrank the post-fix scans by 2:1. The hardware fix appears to reduce cases with local signal loss artifacts in the DWIs, as none were observed post-fix on any of the scanners. Nevertheless, the directional artifacts were still visually and computationally detected in the color-coded FA images, though at reduced rate with 8% of scans for the 6 month old participants, and 21% of scans for the 12 month old participants across sites. This demonstrates that while the Siemens hardware fix definitely reduces the extent of this issue, it does not eliminate its occurrence and thus thorough quality control is still necessary to detect directional artifact.

Dominant direction artifact detection in adult scans

For adult scans, we chose a set of 80 test images acquired as part of the longitudinal TRACK-HD study (Tabrizi et al., 2009). The acquisition protocol employs eight $b = 0$ and 64 gradient directions uniformly spaced with single $b\text{-}value = 1000$ s/mm^2 at a resolution of 2.5 mm isotropic. Fig. 7-a shows whole brain z-scores for these images. For this dataset no information was provided as to whether the original

[4] http://www.ibis-network.org.

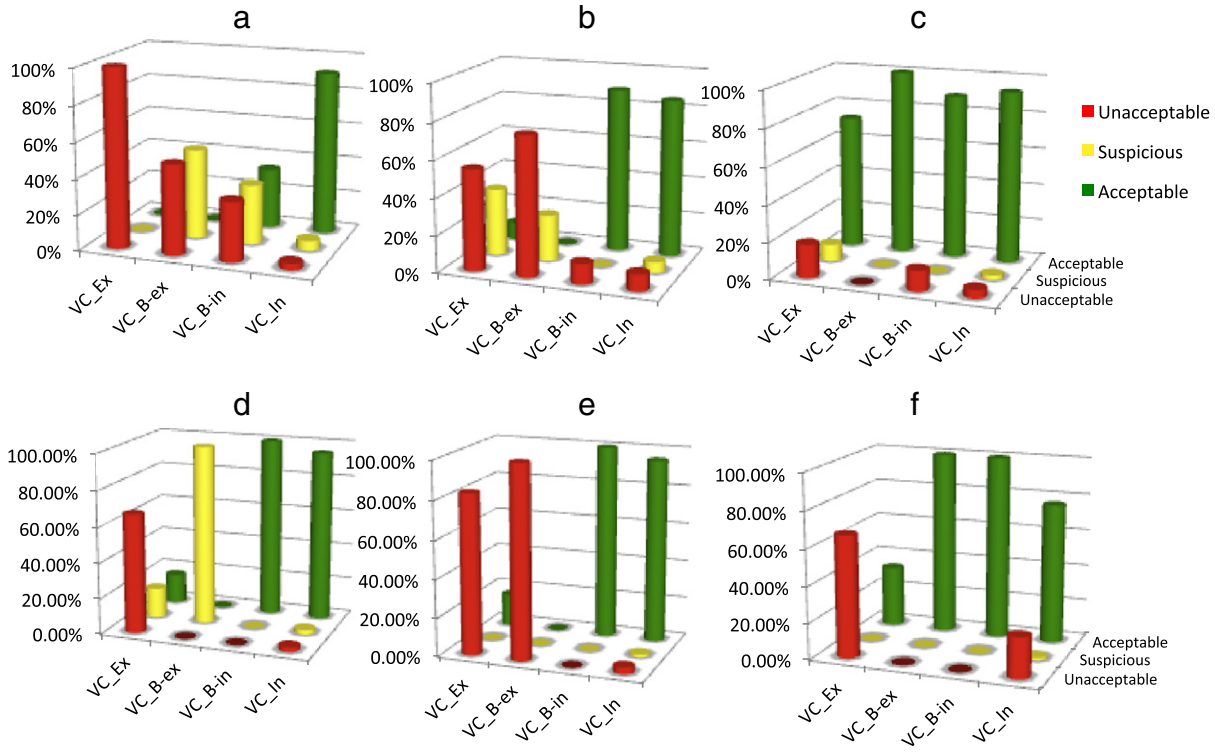

Fig. 6. Detection performance in the pediatric study in subjects 6 (a–c) and 12 months old (d–f): Plots show agreement between visual checking QC based classification into exclude (VC-Ex), borderline exclude (VC-B-ex), borderline include (VC-B-in) and include (VC-In) groups and our detection process on whole brain (a,d), gray matter with CSF (b,e) and white matter regions (c,f). Within the whole brain region (a,d) there is considerable agreement as most excluded cases scored within the unacceptable range. A small set of cases scored within the unacceptable range and was classified as include. The detection results for 12 months are more consistent compared to the 6 months old across the different regions. However, in the white matter region a considerable portion of the data scores within the acceptable range despite a visual exclusion classification. Overall, the agreement is best for the whole brain region for both 6 and 12 months.

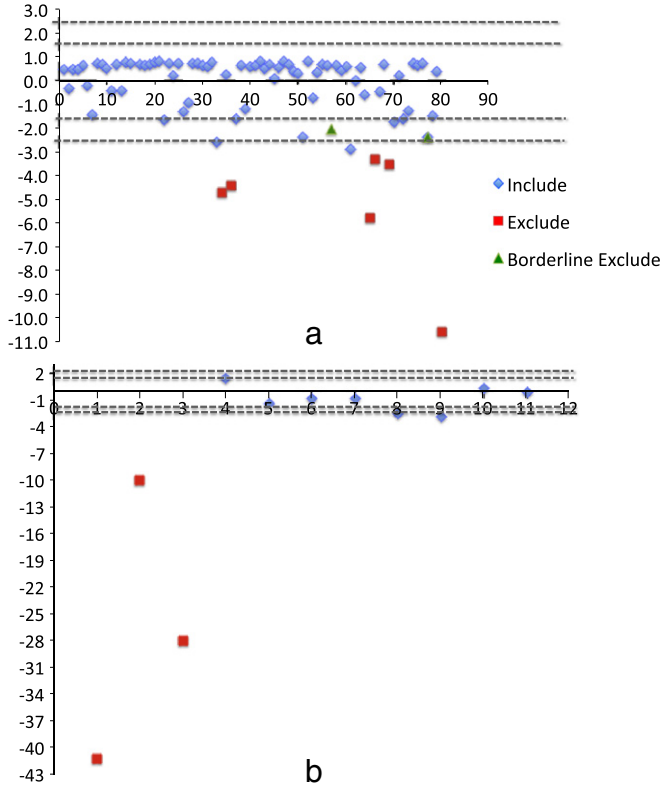

Fig. 7. Plot of whole brain z-scores from adult data (a) and pathology data (b). The dashed lines represent the cutoff of suspicious and unacceptable categories. The x-axis label defines the participant number and the y-axis defines the z-score value.

visual QC checked for dominant direction artifacts. However, upon our visual inspection of the color coded FAs, 6 scans were categorized as affected by severe dominant direction artifacts. We then employed statistical means for training to determine if our detection method could also identify these 6 affected scans. We computed the median overall entropy measurement from the entire set as a robust estimator of the mean entropy. The 16th and 84th percentiles were employed for a robust estimation of the surrogate standard deviation. Our experiments show that our detection method is able to identify all of the scans categorized as “Exclude” and “Borderline Exclude” in the visual QC. However, the quantile based standard deviation is too restrictive as several artifact-free scans were detected as unacceptable.

Dominant direction artifact detection in scans containing pathology

We investigated the capability of our method to detect dominant directional artifacts in subjects with brain pathology. In order to inspect the method in this context, we have used a set of neonates (11 scans) diagnosed with Krabbe disease (Escolar et al., 2009). Fig. 7-b shows the results of these scans. The scans were acquired at 2 mm isotropic resolution and *b-value* = 1000 s/mm^2. While the first 3 scans were obtained by a standard 6 directional ($1 \times b = 0$, NEX 5) DTI protocol, the others were acquired by a uniform 42 directional (with seven $b = 0$ scans, NEX = 1) DTI protocol. We have trained each DWI acquisition scheme separately, using 86 artifact-free scans with 6-DW directions and 56 artifact-free scans with 42-DW directions. Three scans from the 6-DW directions group were identified by our procedure and later visually confirmed to suffer from directional dominant artifacts. Unlike the previously discussed data, these scans showed dominant green-blue artifact in the color-coded FA images. For example, Fig. 8 demonstrates a scan with a dominant green-blue artifact in the color FA images, the

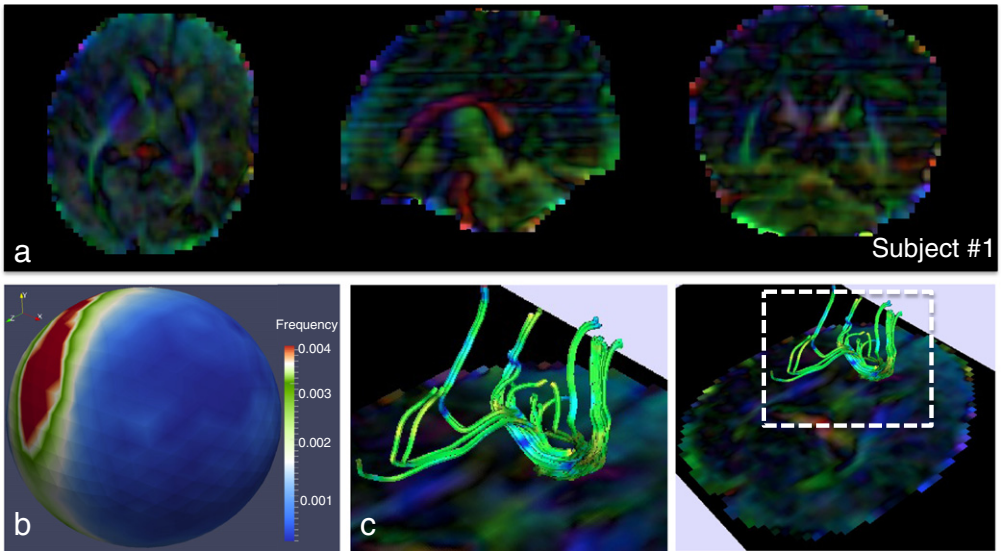

Fig. 8. An example of a Krabbe disease scan disturbed by the dominant green color artifact in axial, sagittal and coronal views, (a), orientational distribution of PD, (b), and tractography of genu fiber bundles, (c). The z-score for this subject is seen as participant #1 in Fig. 7b.

resulting orientational distribution of PDs, and the severely damaged genu fiber bundle tractography.

We have further illustrated the performance of our method in a dataset not suffering from dominant directional artifacts acquired from a patient diagnosed with Grade 4 Glioblastoma. The data were acquired with a 3T GE scanner with 31 gradient directions and one $b = 0$ followed by single *b-value* $= 1000$ s/mm^2. Whole brain coverage was obtained by collecting 52 slices with 1.0 mm voxel size and 2.6 mm slice thickness. We have trained the data using 30 artifact-free scans with 31-DW directions with no pathology acquired on a different type of scanner (3T Siemens Tim Trio) as part of a different study. We resampled this training data to match the testing data resolution. Fig. 12 shows the scan containing a Grade 4 Glioblastoma. The PD distribution of this Glioblastoma containing scan was found to be within acceptable range, which confirmed the visual checking (Fig. 12-d).

Statistical analysis of detection performance

As discussed before, the detection performance of our approach is related to a chosen threshold. In this paper, we use standard Gaussian thresholds to define acceptable, suspicious and unacceptable ranges for our detection approach (acceptable range: $z < 1.64/90\%$, suspicious range: $z \geq 1.64/90\%$ and unacceptable range: $z \geq 2.58/99\%$). In order to analyze the benefits of this threshold compared to other possible thresholds, we have applied a receiver operating characteristic (ROC) analysis. The ROC curves depict relative trade-offs between benefits and costs of a detection method at various threshold settings by plotting the fraction of the true positive rate (sensitivity) and false positive rate (1-specificity). The best possible detection result would yield a point in the upper left corner or coordinate (0,1) of the ROC space. In order to compute the ROC curves, we have considered three different test scenarios: 1) all suspicious cases are scored as in-

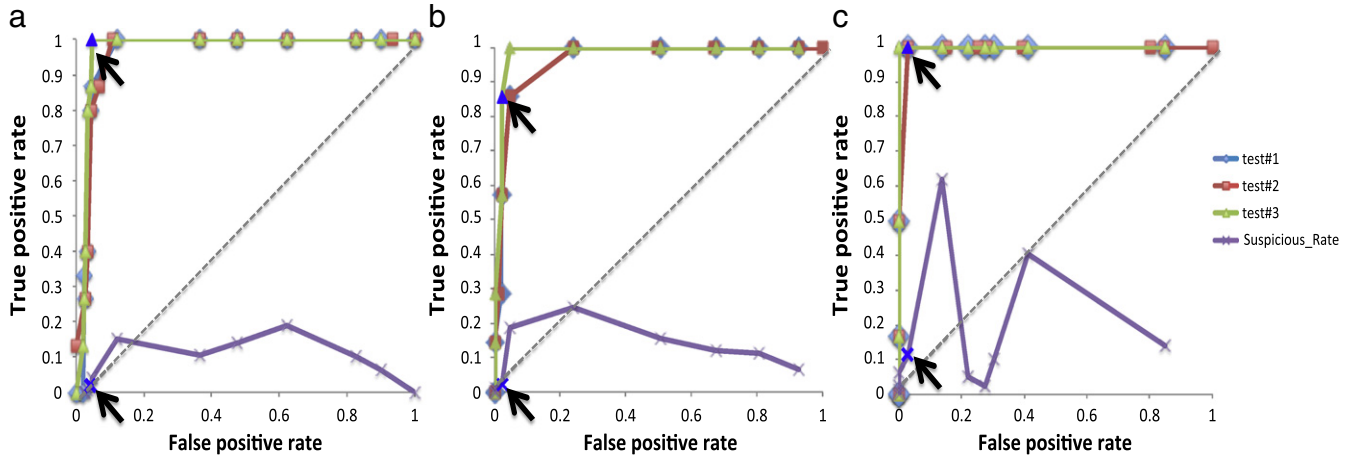

Fig. 9. Receiver operating characteristic curves for pediatric 6 months, 12 months old and adult TRACK-HD (a–c). The ROC curves are created for the three tests. Test #1: the suspicious cases were considered as included, test #2: the suspicious cases were considered as excluded, and test #3: the suspicious cases were determined correctly based on visual assessments. Also, the suspicious rate (the percent data needing visual confirmation) curves are plotted for test #3. The arrows point to the threshold, which is employed in our detection method.

Table 2
The statistical measures (sensitivity and specificity) of Fig. 9 for the threshold applied in this paper. For test #3, the suspicious rate was computed for each set.

Test	(Sensitivity, specificity, suspicious rate)		
	Pediatric 6 mo (IBIS)	Pediatric 12 mo (IBIS)	Adult (TRACK-HD)
#1: suspicious → include	(87%, 95%, –)	(57%, 98%, –)	(100%, 97%, –)
#2: suspicious → exclude	(100%, 89%, –)	(86%, 95%, –)	(100%, 85%, –)
#3: suspicious → correct	(100%, 95%, 4%)	(86%, 98%, 2%)	(100%, 97%, 11%)

cluded (test#1), 2) all suspicious cases are scored as excluded (test#2) and 3) all suspicious cases are scored correctly based on visual assessments. (test#3). Fig. 9 shows the ROC curves of these tests and the suspicious rate curve of test #3 with the arrows pointing to the threshold proposed in this paper. By consulting the ROC curves, it can be seen that the suggested thresholds for all three datasets are close to the optimal thresholds, and the occurrence rates of suspicious images are low. The statistical sensitivity and specificity measures of Fig. 9 for the proposed thresholds are shown in Table 2.

Correction

We performed the proposed correction on all cases categorized as suspicious. Fig. 10 presents an example case from the pediatric 12 participant study that suffers from an intermediate degree of red dominant direction artifact. After correcting the images by excluding the most affected gradients, areas previously containing the red artifact visible improved. Specifically when inspecting the color coded FA images, the cingulum and fornix became more apparent. Fig. 11 shows the assessment of a different case with a minor red dominant direction artifact via fiducial-based single-tensor streamline tractography in 3D Slicer in the splenium tract center, and the improved tractography resulting from our correction method. While these examples demonstrate promising correction results for DTI quality control compared with the original image, it has to be noted that many cases detected with the proposed orientational entropy were not salvageable; only those with intermediate to minor artifacts demonstrated potential for correction.

The comparison results with RESTORE

RESTORE (Chang et al., 2005) is a method proposed to detect and correct DTI artifacts affecting tensor estimation by identifying and excluding voxel-wise potential outliers from datasets. There are clear beneficial effects of employing RESTORE on datasets suffering from a variety of DTI artifacts. Consequently, we performed a comparison study against RESTORE to see whether it can successfully detect and potentially correct the vibration/dominating direction artifacts discussed in this paper.

With respect to artifact detection, we have employed the smaller set of cases from the studies presented before, displaying different levels of the artifacts as well as artifact-free cases. First, using the Redundancy Coefficient (RC) criterion, we could not find any threshold that would be sensitive as a rejection criteria, i.e. no RC threshold value was able to differentiate normal cases from artifact cases. Next, we judged a potential detection via the presence of outlier rich areas within the white and gray matter. The respective results show that while RESTORE detects areas of significant outliers within white matter regions for some datasets with local artifacts in the Excluded and BorderlineExcluded categories, no such regions were detected for any of the global artifact cases in the Excluded and BorderlineExcluded categories, nor for any of the BorderlineIncluded cases.

With respect to artifact correction, the correction results from RESTORE showed no evidence that the artifact has been corrected or even reduced. In fact, RESTORE seemingly worsens the effect, accentuating visually those areas that suffer from the artifact the most, both in local and global artifact cases. RESTORE seems more likely to reject the actual biological data as outliers, especially for datasets with significant dominating directions artifacts in low FA regions such as gray matter, or white matter regions in early postnatal pediatric data.

This result in no way lessens the relevance of RESTORE, it merely shows that it does not serve as an appropriate detection or correction method for the particular artifact discussed here. This is most likely due to the correlated nature of the artifact across DWI images. These vibration/dominating direction artifacts thus result in estimated tensors that do not necessarily exhibit outlier characteristics as detected by RESTORE.

Discussion and conclusion

The dominant directional artifact has been discovered as a serious issue in different types of scanners (Hiltunen et al., 2006; Mohammadi et al., 2010; Müller et al., 2011; Nunes et al., 2011). It is dependent on several hardware-based factors, for example, mechanical resonance of the scanner and defined acquisition parameters. Mostly, the occurrence of this artifact has been reported by Siemens scanner users, which can have a non-negligible effect especially in participants under 30 kg (Liu and Liu, 2011). This artifact appears visually either as localized signal loss in DWIs or as a widespread dominant direction color in the corresponding color-coded FA images. One possible reason for this artifact is the vibration of the patient table. It is reported that the padding used to restrain the subject's head during the scan has reduced the artifact occurrence (Müller et al., 2011). Also, a Siemens hardware fix exists that reduces the rate of the localized signal loss artifact in DWIs. However, significant directional artifacts are still present even

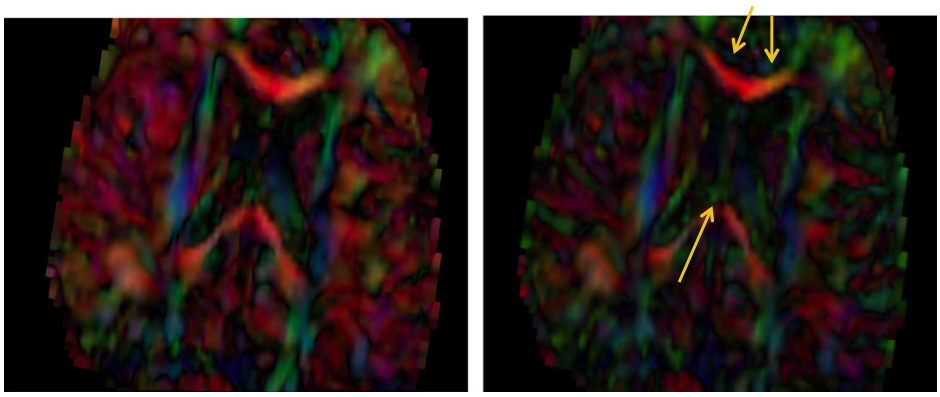

Fig. 10. Improvement in contrast of cingulum and fornix fibers in corrected image (right).

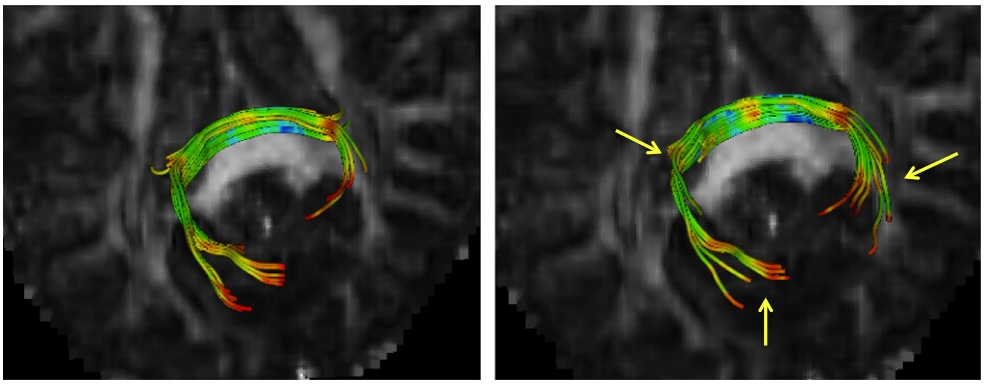

Fig. 11. The fiber tractography of splenium of one of the borderline excluded cases superimposed on a FA image in Fig. 6d before (left) and after (right) our correction step.

after the Siemens hardware fix. While some cases may not have visually apparent signal dropout in the DWIs, as shown by our method, these artifacts become apparent upon visual inspection of the DTIs, specifically the color coded FA images.

This work suggests a method for post-processing detection of the dominant direction artifact via the entropy of the principal direction distribution. We have used the icosahedron subdivision method for computing the PD distribution. While there are other approaches for deriving the samples on the sphere, such as the electrostatic repulsion model Jones et al. (1999), the exact distribution of these bins is not crucial to the work. We have applied the proposed entropy-based detection scheme to numerous scans in a variety of participant populations and compared the findings to the visual assessment by a human expert. Overall, our approach was able to automatically detect the large majority of scans suffering from the residual dominant directional artifacts per visual classification, highlighting the sensitivity of our detection. Table 3 shows the summarized detection performance of our approach for testing experiments based on computed z-score within the whole brain. We also mentioned the occurrence rate for each visual classification. Our proposed method was successful at detecting excluded and borderline excluded scans as suspicious and unacceptable for all of the datasets, except one scan from the pediatric 12 month old study which was scored as acceptable. Nevertheless, a considerable number of datasets were classified as suspicious, for which additional interactive visual checking is necessary.

We have further compared our proposed entropy measure to the residual tensor error metric commonly employed in DWI QC (Tournier et al., 2011). In our experiments, only a small minority of the local signal loss artifacts were detected via residual tensor fit errors. This is likely due to the fact that the vibration leads to a local signal loss that is correlated across the similarly oriented DWIs and thus does not introduce major local errors in the tensor fit metric. Furthermore, statistics using the average tensor fit error across all DWIs did not show any significant difference between artifact-free datasets and those suffering from directional artifacts. Overall, while the residual tensor error metric is a valuable metric for assessing general DWI QC, it does not seem to provide a high potential to detect directional artifacts.

It is noteworthy that if these artifacts are not detected and the corresponding DTI data are not removed from a neuroimaging study, they will introduce a strong bias in the subsequent DTI analysis. Both scalar based applications and tract-based studies will be affected if these artifacts are not detected. We performed an illustrative experiment where we computed the average FA within white matter and gray matter regions for scans that are artifact-free and for scans suffering from the dominant direction artifact. We found that the FA values of artifact rich scans are significantly larger, as their mean values were fully outside the range of the mean FA of artifacts-free scans. These findings clearly show that using scans affected by these artifacts would significantly distort/falsify DTI studies; in both tract-based studies and scalar-based group comparison studies.

The pediatric data experimental results show that the optimal entropy measurements are best computed within the whole brain mask compared to the gray matter mask including CSF, and the white matter mask, at least for pediatric data. In this paper, we have applied tissue segmentation mapping to the average baseline images. Although the registration of tissue segmentation mapping to diffusion images may yield more consistent detection results, the detection performance depends on the correction of susceptibility distortions in the DWIs.

Not surprisingly, the training process is crucial for the accuracy of our dominant direction artifact detection method. Inadequate training will lead to significant performance reduction in the detection, as indicated in our neonate results (see Fig. 7b). The training process is used to compute estimates for the expected distribution of PD from artifact-free data. These trained entropy values are relatively sensitive to certain population properties; in particular, the white matter maturation level and the relative resolution of white matter voxels directly influence the underlying orientation distribution and therefore the entropy. This means that populations with considerably different brain size and/or maturation levels (e.g. neonate vs. 1 year old vs. adult) would need separately trained entropy threshold settings. If possible, we suggest using the same DTI acquisition protocol for the training and target data, especially for DTI acquisition protocols with a low number of gradient directions. Using the same acquisition protocol for training and target data is less

Table 3
Summary of detection performance of our approach based on computed z-score within whole brain region.

	Visual-exclude	Visual-borderline-exclude	Visual-borderline-include	Visual-include
Pediatric 6 mo (IBIS)				
Occurrence rate	4%	1.5%	3.3%	91.2%
Acceptable	0%	0%	33.33%	91.10%
Suspicious	0%	50%	33.33%	5.40%
Unacceptable	100%	50%	33.33%	3.60%
Pediatric 12 mo (IBIS)				
Occurrence rate	6.7%	1.1%	2.2%	90.0%
Acceptable	16.66%	0%	100%	95%
Suspicious	16.66%	100%	0%	2.5%
Unacceptable	66.66%	0%	0%	2.5%
Adult (TRACK-HD)				
Occurrence rate	7.6%	2.5%	–%	89.9%
Acceptable	0%	0%	–%	88.88%
Suspicious	0%	100%	–%	8.33%
Unacceptable	100%	0%	–%	2.77%

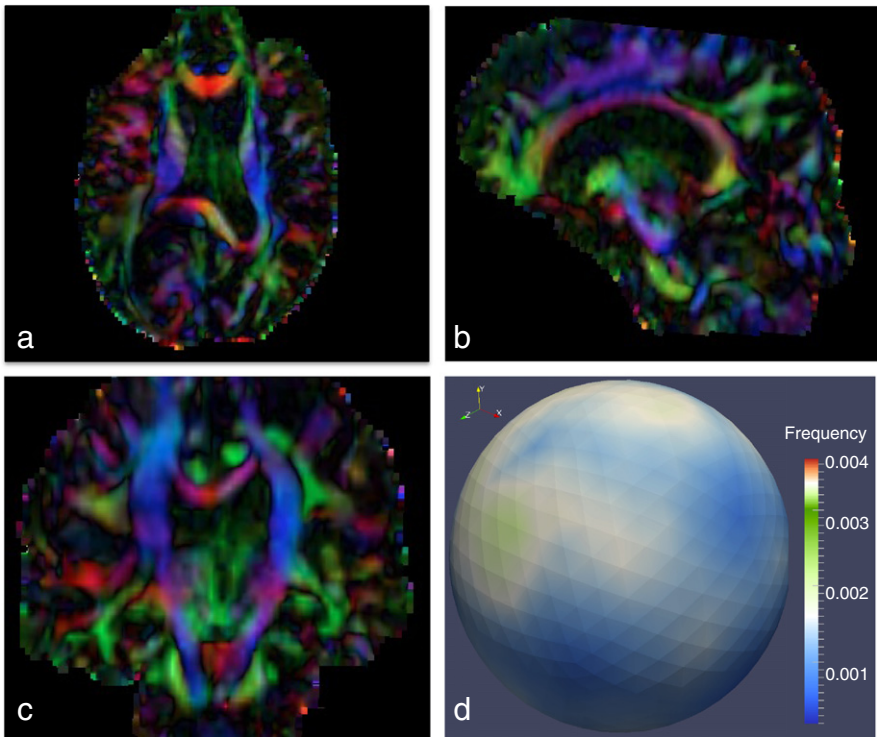

Fig. 12. Brain tumor patient Glioblastoma Grade 4. The color-FA image displaying no dominant directional artifacts, (a–c), along with spherical histogram of the PD distribution within the entire brain, (d). The computed z-score is 0.38, which located in the acceptable range. This example shows that the DT-QC entropy approach does not introduce any bias in the detection of the dominant directional artifacts for this patient.

important in studies collecting more than 20 uniformly distributed gradient directions (Jones, 2004). Also, artifact detection performance can differ based on the number of artifact free scans used in the training process. Using a leave-N-out strategy with 50 repetitions, computed for each dataset (pediatric 6 months, 12 months and adult data), we found no difference in the obtained true positive and true negative rates of detection performance.

It is important to investigate the effect of the dominant directional artifacts on clinical diagnoses based on DWIs. If the affected regions from the artifacts overlap with pathology, the diagnostic confidence will be decreased. In the experimental results, we show a set of neonates (11 scans) with Krabbe disease. Among these scans, our approach successfully detected 3 scans that suffer from dominant directional artifacts (see Fig. 8 as an example). All other Krabbe datasets without visually detectable artifacts are scored as acceptable. In addition, we investigated data acquired from a patient diagnosed with Grade 4 Glioblastoma. The dataset displayed no artifacts, and was scored within acceptable range (see Fig. 12). These results indicate that the PD distribution, and thus the ability to detect directional artifacts is not affected by these brain pathologies. One concern to acknowledge is the potential risk for bias to be introduced for group comparisons in studies looking at different brain pathologies if directional artifacts occur more frequently in the pathology group.

We propose a correction approach that refurbishes DWIs by excluding gradients most affected by vibrational artifacts using the entropy measurement. The exclusion continues until the computed z-score reaches an acceptable value, or the number of excluded gradients can be set by default. We have applied our correction method on exclude and borderline exclude cases for pediatric and adult datasets. The result was that only borderline exclude cases were salvaged after correction; we were not able to salvage the other exclude cases after correction, in terms of visual assessment of the color coded FA images. After correction, the improvement of borderline exclude cases is evident in both assessment of color coded FA images and fiber analysis. Thus, this approach has the potential to correct images suffering from mild to moderate artifacts. We believe that other outlier rejection methods, such as Robust Estimation of Tensors by Outlier Rejection (RESTORE) (Chang et al., 2005) and Higher Order Model Outlier Rejection (HOMOR) Pannek et al. (2012), can be used to improve our correction approach. This improvement is important for fiber crossing and high b-value ($b = 3000$ s/mm^2) situations. We are currently continuing research in this direction.

The entropy based DTI QC presented in this paper has been included within the open-source DTIPrep tool.[5] Expected runtime on a standard workstation is about 15 min with 2–3 min for the tensor estimation and our entropy based QC of the principal orientation distribution.

Acknowledgment

The Infant Brain Imaging Study (IBIS) Network is an NIH-funded Autism Center of Excellence HD-055741 and HD-003110 and consists of a consortium of seven universities in the United States and Canada. Clinical sites are located at the University of North Carolina (J. Piven, IBIS Network primary investigator; H.C. Hazlett, C. Chappell); the University of Washington (S.R. Dager, A.M. Estes, D. Shaw); Washington University (K.N. Botteron, R.C. McKinstry, J. Constantino, J. Pruett); the Childrens Hospital of Philadelphia (R.T. Schultz, S.J. Paterson); and the University of Alberta (L. Zwaigenbaum). The data coordinating center is at the Montreal Neurological Institute (A.C. Evans, D.L. Collins, G.B. Pike, V. Fonov, P. Kostopoulos, S. Das). The image processing core is at the University of Utah (G. Gerig) and the University of North Carolina (M. Styner). The statistical analysis core is at the University of North Carolina (H. Gu). The genetics analysis core is at the University of North Carolina (P. Sullivan, F. Wright).

[5] http://www.nitrc.org/projects/dtiprep/.

Additional support is provided by the following grants: NIH grants P50 MH 064065, MH070890, P30 HD03110, R01 MH091645, U54 EB005149-01 (NA-MIC), R01 NS061965, and P01-DA022446, as well as by the Track-HD project funded by the CHDI/High Q Foundation.

Conflict of interest

None.

References

Andersson, J., Skare, S., 2002. A model-based method for retrospective correction of geometric distortions in diffusion-weighted EPI. NeuroImage 16 (1), 177–199.
Andersson, J., Skare, S., Ashburner, J., 2003. How to correct susceptibility distortions in spin-echo echo-planar images: application to diffusion tensor imaging. NeuroImage 20 (2), 870–888.
Bach, D., Behrens, T., Garrido, L., Weiskopf, N., Dolan, R., 2011. Deep and superficial amygdala nuclei projections revealed in vivo by probabilistic tractography. J. Neurosci. 31 (2), 618–623.
Basser, P., Mattiello, J., Lebihan, D., et al., 1994. Estimation of the effective self-diffusion tensor from the NMR spin echo. J. Magn. Reson. - Ser. B 103 (3), 247–254.
Basser, P., Pajevic, S., Pierpaoli, C., Duda, J., Aldroubi, A., 2000. In vivo fiber tractography using DT-MRI data. Magn. Reson. Med. 44 (4), 625–632.
Chang, L., Jones, D., Pierpaoli, C., 2005. Restore: robust estimation of tensors by outlier rejection. Magn. Reson. Med. 53 (5), 1088–1095.
Clarke, K., 2002. Criteria and measures for the comparison of global geocoding systems. Discrete Global Grids: A Web Book.University of California, Santa Barbara (http://www.ncgia.ucsb.edu/globalgrids-book).
Cui, J., Wen, C., Hu, Y., Mak, K., Mak, K., Luk, K., 2011. Orientation entropy analysis of diffusion tensor in healthy and myelopathic spinal cord. NeuroImage 58 (4), 1028–1033.
Escolar, M., Poe, M., Smith, J., Gilmore, J., Kurtzberg, J., Lin, W., Styner, M., 2009. Diffusion tensor imaging detects abnormalities in the corticospinal tracts of neonates with infantile Krabbe disease. Am. J. Neuroradiol. 30 (5), 1017–1021.
Fillard, P., Pennec, X., Arsigny, V., Ayache, N., 2007. Clinical DT-MRI estimation, smoothing, and fiber tracking with log-Euclidean metrics. Med. Imaging IEEE Trans. 26 (11), 1472–1482.
Gallichan, D., Scholz, J., Bartsch, A., Behrens, T., Robson, M., Miller, K., 2010. Addressing a systematic vibration artifact in diffusion-weighted MRI. Hum. Brain Mapp. 31 (2), 193–202.
Hiltunen, J., Hari, R., Jousmäki, V., Müller, K., Sepponen, R., Joensuu, R., 2006. Quantification of mechanical vibration during diffusion tensor imaging at 3T. NeuroImage 32 (1), 93–103.
Hsu, J., Leemans, A., Bai, C., Lee, C., Tsai, Y., Chiu, H., Chen, W., 2008. Gender differences and age-related white matter changes of the human brain: a diffusion tensor imaging study. NeuroImage 39 (2), 566–577.
Jezzard, P., Clare, S., et al., 1999. Sources of distortion in functional MRI data. Hum. Brain Mapp. 8 (2–3), 80–85.
Johansen-Berg, H., Rushworth, M., 2009. Using diffusion imaging to study human connectional anatomy. Annu. Rev. Neurosci. 32, 75–94.
Jones, D., 2004. The effect of gradient sampling schemes on measures derived from diffusion tensor MRI: a Monte Carlo study. Magn. Reson. Med. 51 (4), 807–815.
Jones, D., Horsfield, M., Simmons, A., 1999. Optimal strategies for measuring diffusion in anisotropic systems by magnetic resonance imaging. Magn. Reson. Med. 42.
Le Bihan, D., Breton, E., Lallemand, D., Grenier, P., Cabanis, E., Laval-Jeantet, M., et al., 1986. MR imaging of intravoxel incoherent motions: application to diffusion and perfusion in neurologic disorders. Radiology 161 (2), 401.
Liu, K., Liu, X., Apr. 12 2011. Vibrationally decoupled patient table for use in magnetic resonance system. US Patent 7,924,008.
Liu, Z., Wang, Y., Gerig, G., Gouttard, S., Tao, R., Fletcher, T., Styner, M., 2010. Quality control of diffusion weighted images. Society of Photo-Optical Instrumentation Engineers (SPIE) Conference Series 7628, 17.
Mohammadi, S., Deppe, M., Möller, H., 2010. Scaling in readout direction: a vibration-induced distortion of diffusion-weighted images and its retrospective correction by affine registration. Proc Intl Soc Magn Reson Med, vol. 18, p. 3103.
Mohammadi, S., Nagy, Z., Hutton, C., Josephs, O., Weiskopf, N., 2011. Correction of vibration artifacts in DTI using phase-encoding reversal (COVIPER). Magn. Reson. Med. 68 (3), 882–889.
Mori, S., Crain, B., Chacko, V., Van Zijl, P., 1999. Three-dimensional tracking of axonal projections in the brain by magnetic resonance imaging. Ann. Neurol. 45 (2), 265–269.
Mukherjee, P., Chung, S., Berman, J., Hess, C., Henry, R., 2008. Diffusion tensor MR imaging and fiber tractography: technical considerations. Am. J. Neuroradiol. 29 (5), 843–852.
Müller, H., Glauche, V., Novak, M., Nguyen-Thanh, T., Unrath, A., Lahiri, N., Read, J., Say, M., Tabrizi, S., Kassubek, J., et al., 2011. Stability of white matter changes related to Huntingtons disease in the presence of imaging noise: a DTI study. PLos Curr. 3.
Nunes, R., Malik, S., Hajnal, J., 2011. Prospective correction of spatially non-linear phase patterns for diffusion-weighted fse imaging using tailored rf excitation pulses. 19th Annual Proceedings of the ISMRM, Montreal, Quebec, Canada, p. 172.
Pannek, K., Raffelt, D., Bell, C., Mathias, J.L., Rose, S.E., 2012. Homor: higher order model outlier rejection for high b-value MR diffusion data. NeuroImage 63 (2), 835–842 (URL http://www.sciencedirect.com/science/article/pii/S1053811912007331).
Pierpaoli, C., Basser, P., 1996. Toward a quantitative assessment of diffusion anisotropy. Magn. Reson. Med. 36 (6), 893–906.
Prastawa, M., Gilmore, J., Lin, W., Gerig, G., 2005. Automatic segmentation of MR images of the developing newborn brain. Med. Image Anal. 9 (5), 457–466.
Reese, T., Heid, O., Weisskoff, R., Wedeen, V., 2003. Reduction of eddy-current-induced distortion in diffusion mri using a twice-refocused spin echo. Magn. Reson. Med. 49 (1), 177–182.
Salvador, R., Pena, A., Menon, D., Carpenter, T., Pickard, J., Bullmore, E., 2005. Formal characterization and extension of the linearized diffusion tensor model. Hum. Brain Mapp. 24 (2), 144–155.
Shannon, C., 2001. A mathematical theory of communication. ACM SIGMOBILE Mob. Comput. Commun. Rev. 5 (1), 3–55.
Solano-Castiella, E., Anwander, A., Lohmann, G., Weiss, M., Docherty, C., Geyer, S., Reimer, E., Friederici, A., Turner, R., 2010. Diffusion tensor imaging segments the human amygdala in vivo. NeuroImage 49 (4), 2958–2965.
Tabrizi, S., Langbehn, D., Leavitt, B., Roos, R., Durr, A., Craufurd, D., Kennard, C., Hicks, S., Fox, N., Scahill, R., et al., 2009. Biological and clinical manifestations of huntington's disease in the longitudinal track-hd study: cross-sectional analysis of baseline data. Lancet Neurol. 8 (9), 791–801.
Tournier, J., Mori, S., Leemans, A., 2011. Diffusion tensor imaging and beyond. Magn. Reson. Med. 65 (6), 1532–1556.
Tristán-Vega, A., Aja-Fernández, S., 2010. DWI filtering using joint information for DTI and HARDI. Med. Image Anal. 14 (2), 205–218.
Unrath, A., Müller, H., Riecker, A., Ludolph, A., Sperfeld, A., Kassubek, J., 2010. Whole brain-based analysis of regional white matter tract alterations in rare motor neuron diseases by diffusion tensor imaging. Hum. Brain Mapp. 31 (11), 1727–1740.
Wang, Z., Vemuri, B., Chen, Y., Mareci, T., 2004. A constrained variational principle for direct estimation and smoothing of the diffusion tensor field from complex DWI. Med. Imaging IEEE Trans. 23 (8), 930–939.